Article

A Three-Zone Scavenging Model for Large Two-Stroke Uniflow Marine Engines Using Results from CFD Scavenging Simulations

Michael I. Foteinos [1,*] **, Alexandros Papazoglou** [1]**, Nikolaos P. Kyrtatos** [1]**,
Anastassios Stamatelos** [2,*] **, Olympia Zogou** [2] **and Antiopi-Malvina Stamatellou** [2]

[1] Laboratory of Marine Engineering, National Technical University of Athens, GR-15780 Athens, Greece;
apapazo2006@gmail.com (A.P.); nkyrt@lme.ntua.gr (N.P.K.)
[2] Laboratory of Thermodynamics & Thermal Engines, University of Thessaly, GR-38334 Volos, Greece;
olyz@uth.gr (O.Z.); malvinstam@gmail.com (A.-M.S.)
[*] Correspondence: m.foteinos@lme.ntua.gr (M.I.F.); stam@uth.gr (A.S.)

Abstract: The introduction of modern aftertreatment systems in marine diesel engines call for accurate prediction of exhaust gas temperature, since it significantly affects the performance of the aftertreatment system. The scavenging process establishes the initial conditions for combustion, directly affecting exhaust gas temperature, fuel economy, and emissions. In this paper, a semi-empirical zero-dimensional three zone scavenging model applicable to two-stroke uniflow scavenged diesel engines is updated using the results of CFD (computational fluid dynamics) simulations. In this 0-D model, the engine cylinders are divided in three zones (thermodynamic control volumes) namely, the pure air zone, mixing zone, and pure exhaust gas zone. The entrainment of air and exhaust gas in the mixing zone is specified by time varying mixing coefficients. The mixing coefficients were updated using results from CFD simulations based on the geometry of a modern 50 cm bore large two-stroke marine diesel engine. This increased the model's accuracy by taking into account 2-D fluid dynamics phenomena in the cylinder ports and exhaust valve. Thus, the effect of engine load, inlet port swirl angle and partial covering of inlet ports on engine scavenging were investigated. The three-zone model was then updated and the findings of CFD simulations were reflected accordingly in the updated mixing coefficients of the scavenging model.

1. Introduction

During the scavenging process, the burnt gas inside the engine cylinders is expelled and new fresh air is charged. The scavenging process establishes the initial conditions of the combustion process, hence is affecting engine fuel economy and emissions. Commercial vessels, such as tankers, bulk carriers, and containerships are, in most cases, propelled by large two-stroke uniflow scavenged diesel engines. Better propulsion efficiency dictates the matching of the engine to a slow turning, large diameter propeller. In order to achieve low engine revolutions while maintaining a certain mean piston speed the bore to stroke ratio of marine diesel engines was increased. Due to their long stroke, loop or cross flow scavenging was unsuitable for these engines and the uniflow scavenging system was introduced. The air enters the engine cylinders through ports located at the lower part of the liner, when the piston is near the bottom dead center (BDC). After exhaust blowdown the incoming air expels the exhaust gas through the exhaust valve located on the cylinder head. The driving force of the scavenging process is the pressure difference between the scavenge receiver and the exhaust gas

receiver. Inlet ports are usually angled, providing the incoming air with swirl to improve purging of the cylinder. A cross sectional view of a typical large uniflow scavenged marine diesel engine is shown in Figure 1.
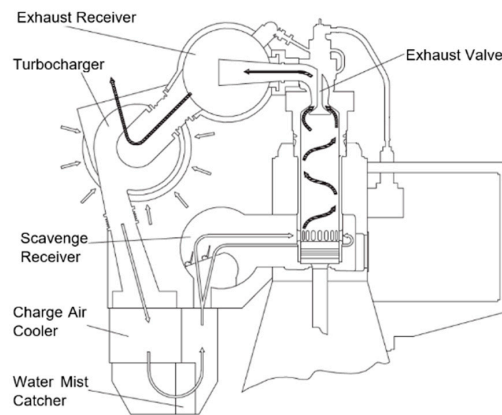
Figure 1. Cross sectional view of a uniflow scavenged marine diesel engine [1].

Before CFD models became widely available the scavenging process was investigated in detail by experiments in scaled down engine models. Such works include visualization, pitot tube measurements, and hot wire experiments which can be found in [2–4]. The effect of inlet port angle on scavenging efficiency was investigated in [5,6]. A review of the various models of the scavenging process can be found in [7,8].

Over the past two decades computational cost has declined leading to increased popularity of CFD modeling. Sigurdson et al., performed a CFD analysis, on a 12-degree sector, including one scavenge port, of the MAN B&W 4T50 test engine (MAN B&W, Copenhagen, Denmark) [9]. Lamas et al. [10] investigated the scavenging process in the MAN B&W 7S50-MC engine (MAN B&W, Copenhagen, Denmark) through CFD simulations. Andersen et al. performed CFD investigation on full scale engines, examining the effect of engine load [11] and variation of in-cylinder swirl [12] on scavenging efficiency. The effect of inlet port depth on the swirling flow and scavenging process was investigated by [13]. The effect of piston covering half of the inlet ports on the in-cylinder swirling flow was examined by [14].

As the bore to stroke ratio of marine engines increased, zonal models became preferable for accurate engine performance prediction. A three-zone scavenging submodel was originally introduced in [15]. Due to the introduction of aftertreatment technologies in marine diesel engines such as selective catalytic reduction (SCR) systems, accurate exhaust gas temperature prediction became more essential. Hence, the original three-zone scavenging model was updated using results from CFD simulations. The updated model can be used in conjunction with a zero-dimensional engine and SCR model, in order to investigate the transient response of the engine-SCR system.

2. The Three-Zone Scavenging Model

In the original model [15], the cylinder is divided in three zones namely, a pure air zone, a pure exhaust gas zone, and a mixing zone as presented in Figure 2.

Within each zone the temperature is assumed uniform but differs in the three zones. The pressure throughout the cylinder is uniform at each computational step. Every zone is treated as an open system where the first law of thermodynamics may be applied.

$$-p\dot{V} + \sum_{sf} \dot{Q}_{sf} + \sum_{j} h_j \dot{m}_j = \frac{d}{dt}(mu) \tag{1}$$

where p is gas pressure, $\dot{V}$ is the rate of change of gas volume, $\dot{Q}$ is the rate of change of heat, h is enthalpy, $\dot{m}$ is rate of change of mass and u is internal energy of the gas. An important assumption

of this three-zone model is that the mass exchange between the zones takes place only in two ways: scavenge air enters the mixing zone and burnt gas enters the mixing zone. Hence the rate of change of the mas for each zone is defined as:

$$\dot{m}_I = \dot{m}_{inp} - \dot{m}_{I-II} \tag{2}$$

$$\dot{m}_{II} = \dot{m}_{I-II} + \dot{m}_{III-II} \tag{3}$$

$$\dot{m}_{III} = -\dot{m}_{III-II} - \dot{m}_{exv} \tag{4}$$

where $\dot{m}_{I-II}$ is the air mass flow rate from zone I to zone II, $\dot{m}_{inp}$ is the air mass flow through inlet ports, $\dot{m}_{III-II}$ is the mass flow rate from zone III to zone II and $\dot{m}_{exv}$ is the mass flow rate through the exhaust valve. The entrainment of air and exhaust gas in the mixing zone is specified by time varying mixing coefficients. The air penetration coefficient is defined as:

$$\mu_a = \frac{\dot{m}_{I-II}}{\dot{m}_{inp}} \tag{5}$$

And the exhaust gas penetration coefficient is defined as:

$$\mu_g = \frac{\dot{m}_{III-II}}{\dot{m}_{inp}}. \tag{6}$$

where $\dot{m}_{III-II}$ is the air mass flow rate from zone III to zone II. The postulated variation of the air penetration coefficient is shown in Figure 3.
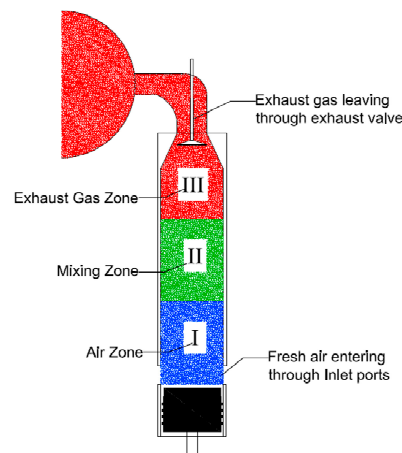

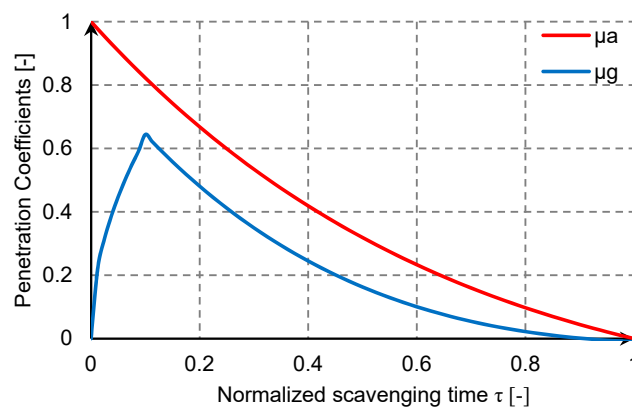**Figure 2.** Schematic representation of the three-zone model on a uniflow scavenged engine.

Figure 3. Variation of μ_α and μ_g at the original model.

Initially, $\mu_\alpha = 1$ since the air entering the engine cylinders is rapidly mixed with exhaust gases. As the exhaust gas in the lower part of the cylinder is displaced, the value of the coefficient declines exponentially, as Equation (7) shows.

$$\mu_\alpha = e^{-\kappa\tau}(\lambda\tau + 1) \tag{7}$$

where κ is a model constant and τ is normalized scavenging time defined as:

$$\tau = \frac{\varphi - \varphi_{EBF}}{\varphi_{IPC} - \varphi_{EBF}} \tag{8}$$

where φ is crank angle, φ_{EBF} is the crank angle at end of backflow and φ_{IPC} is the crank angle at inlet port closing. The assumed variation of μ_g is divided in two phases and is also presented in Figure 3. Initially, $\mu_g = 0$ and increases parabollicaly, resembling the entrainment of ambient fluid into jets. In the second mixing phase, the gas penetration coefficient decreases exponentially. The mathematical expression of μ_g is shown in Equation (9).

$$\mu_g = \begin{cases} 2\sqrt{\tau}, & 0 < \tau < \tau_g{}^* \\ e^{-k(\tau_2)}\left(\xi\tau_2 + \mu_g\left(\tau_g{}^*\right)\right), & 0 < \tau_2 < 1 \end{cases} \tag{9}$$

where ξ and k are model parameters, $\tau_g{}^*$ is the time when the second mixing phase begins and τ_2 is normalized scavenging time of the second mixing phase.

3. Scope of Work

In this paper, the three-zone scavenging model, originally presented in [15] and applicable to two-stroke uniflow scavenged marine diesel engines is updated. The model has been used for many years, in conjunction with a control volume, zero-dimensional engine simulation code, MOTHER (MOtor THERmodynamics) (see Chapter 3). A reliable scavenging model is essential for accurate exhaust gas temperature prediction in engine application. This has become even more important due to the recent applications of DeNOx systems such as SCR [16], exhaust gas recirculation (EGR) [17], and WaCoReG system [18].

Available data concerning the scavenging process of two-stroke engines are scarce compared to four-stroke engines due to the large cost associated with large engine testing and the limited number of test facilities for large engines. To update the original zero-dimensional scavenging model, results from a CFD simulation of the scavenging process were used as baseline. The engine geometry used for this study is from a MAN 50 cm bore size two-stroke marine engine. The specifications of the engine are presented in Table 1.

Table 1. Engine specifications.

Engine Model	MAN B&W 6S50ME	
Bore	500	mm
Stroke	2000	mm
No. of Cylinders	6	-
P_{MCR}	7620	kW
N_{MCR}	115	RPM
Scavenging	Uniflow	
Ports per cylinder	30	

CFD results were produced for four steady state load points along a propeller curve namely 25%, 50%, 75%, and 100%, for two different cases. In the first case inlet ports were fully uncovered by the piston and port angle varied from 0° to 30° by 10° intervals. In the second case port angle was fixed at

20° and a 5% and 10% covering of the inlet port area by the piston at BDC was investigated. Then, the mixing coefficients of the three-zone model were revised using the results from the CFD simulations.

4. The Zero-Dimensional Engine Simulation Code

The scavenging model under consideration, is integrated in the NTUA in-house thermodynamic engine prediction code MOTHER. The code is based on the control volume principle. A number of basic engineering elements such as flow receivers (cylinders, plenums), flow controllers (valves, compressors, turbines), and mechanical elements (shafts, gearboxes, clutches and shaft loads) are available. A turbocharged engine can be modelled as several flow receiver elements interconnected by flow controller elements. Flow receivers are treated as open thermodynamic systems and the work, heat and mass transfer, which take place through their boundaries, are calculated by applying the conservation equations in appropriate form to each control volume. The resulting set of differential equations are numerically solved step-by-step for all volumes. MOTHER includes a variety of submodels for the simulation of engine processes such as combustion, heat transfer, friction, and scavenging. The MOTHER code has been used for many years in engine performance simulations [19–22].

5. Implementation of the CFD Model

To update the mixing coefficients of the original three-zone model results from a more detailed 2D CFD model were used. Only the scavenging process (not the combustion) was simulated. The simulation is carried out between 76–286 CA degrees, for one typical cylinder. The starting point of the simulation (76 crank angle degrees (CAD)) is well before the uncovering of inlet ports by the piston which takes place at 135 CAD. This was done in order to include the blowdown period in the simulation and be able to validate the CFD model against available pressure diagrams. Convective heat transfer in the cooled upper part of the cylinder and the cylinder head is modeled with the assumption of a constant wall temperature. Piston and lower cylinder liner part cooling was not taken into account.

The turbulent flow was simulated by the RANS (Reynolds averaged Navier Stokes) equations [23]. Gas density was calculated using the ideal gas equation. The turbulent viscosity was modeled by the RNG k-ε model [24]. The case is solved in Fluent software as 2-D, axisymmetric with swirl. The bending of the exhaust pipe to enter the receiver is not taken into account and inlet ports are modeled as a continuous opening in the cylinder wall.

Mesh generation was carried out in ICEM CFD software (v14.5) [25] (structured mesh). Only the cylinder, intake ports, and exhaust duct were meshed. Quad elements were employed in the mesh generation. The mesh movement was imposed to the valve and piston surfaces by means of the "in-cylinder" dynamic mesh facility existing in Fluent software [26]. Turbulent heat transport was modeled using Reynolds analogy. Gas components were computed by a species transport model. The number of elements varied from about 17,000 at the starting point of the simulation (76 degrees ATDC, about mid-stroke) to 30,000 at bottom dead center. Figure 4 shows a cross-section of the mesh at 76 CA degree and 180 CA degree.
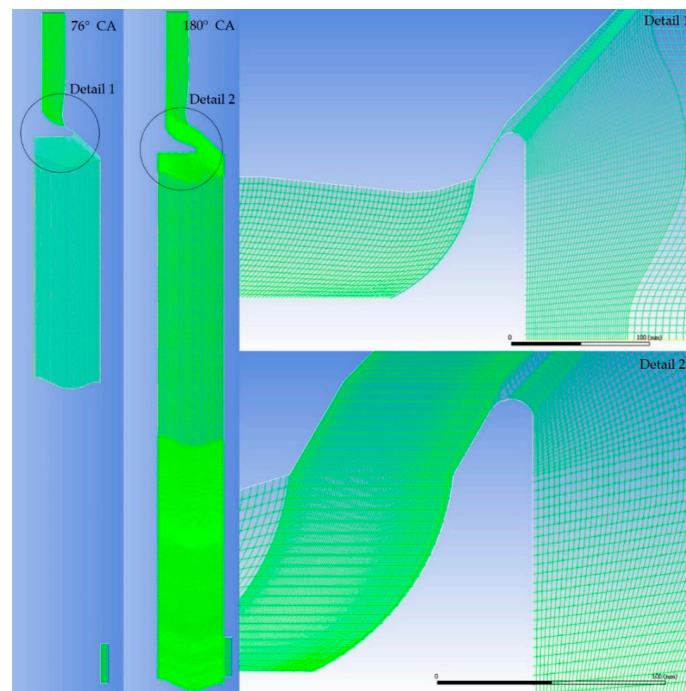
Figure 4. Computational mesh at 76 crank angle degrees (CAD)—180 CAD.

5.1. Numerical Procedure

The PISO (Pressure Implicit with Splitting of Operators) algorithm was chosen for pressure-velocity coupling [26]. A second order scheme was selected to discretize the continuity, momentum, energy and mass fraction equations. The time derivatives were discretized through a first order fully implicit scheme with a constant time step corresponding to 0.1 degrees crank angle.

5.2. Initial and Boundary Conditions—Validation

The flow through the inlet ports was assumed fully axisymmetric, with a radial and a tangential component (swirl). A pressure boundary condition was employed at engine inlet. A turbulence intensity of 5% was selected. The inlet air temperature and CO_2 concentration were set at 313 K and 0% respectively. A pressure boundary condition was employed at engine outlet. Initial conditions for the gas in the cylinder (76° CA) are shown in Table 2. They were produced using the zero-dimensional, engine performance prediction code MOTHER [19]. The engine under consideration was modelled under steady conditions using the MOTHER software and validated against available measured data. After submodel calibration, the accuracy of MOTHER calculations against measured data is better than 3% over the whole operating range of an engine and it has been validated with over 50 engine types [27–29].

Table 2. Initial conditions for the CFD model.

Engine Load	100%	75%	50%	25%
N [RPM]	115.3	105	91.5	73
p_{cyl} at 76° CA [bar]	14.8	11.7	8.81	5.6
T_{cyl} at 76° CA [K]	1239	1186	1163	1020
p_{scav} [bar]	3.90	3.15	2.20	1.48
p_{exh} [bar]	3.80	3.08	2.15	1.45
CO_2 mass fraction	0.133	0.129	0.129	0.115
H_2O mass fraction	0.049	0.0475	0.0475	0.0423
Air mass fraction	0.358	0.376	0.376	0.444

The comparison of engine indicator diagrams with the average pressure computed by the CFD model is a good overall check of the CFD model's accuracy. In this study the CFD computed pressure diagram compares well with the validated 0-D model, for the engine cycle part of the CFD computation (76–286 degrees CA) for all four operation points (25–100% load, along the propeller curve). The flow through the cylinder is driven by a pressure difference between the scavenge receiver and the exhaust receiver, known as the scavenging gradient or Δp across engine. Higher dimension CFD models with advanced turbulence submodels may require a certain degree of correction of scavenging gradient by modification of the mass flow-rate [30]. In the present case the exhaust receiver pressure as well as the inlet pressure are given as boundary conditions and thus the mass flow-rate is computed. Figure 5 shows the effect of the scavenging gradient on some important scavenging parameters, namely, trapping efficiency (η_{tr}), charging efficiency (η_{ch}), scavenging efficiency (η_{sc}), massflow of air entering the cylinders ($\dot{m}_{inp}$), and the mass of delivered air retained ($m_{air,ret}$). The definition of each efficiency is given below:

$$\eta_{tr} = \frac{m_{air,ret}}{m_{air,del}} \tag{10}$$

$$\eta_{ch} = \frac{m_{air,ret}}{V_{ref} \cdot \rho_{inl}} \tag{11}$$

$$\eta_{sc} = \frac{m_{air,ret}}{m_{tr}} \tag{12}$$

where $m_{air,del}$ is the mass of delivered air, V_{ref} is the reference cylinder volume, ρ_{inl} is the density at the engine inlet and m_{tr} is the mass of the total trapped cylinder charge.

As shown in Figure 5 the CFD model is sensitive to the scavenging gradient and the mass flow-rate is computed correctly without any corrections needed. The trapping efficiency and the air mass flow rate through the inlet ports are the most affected quantities by a change in Δp. Thus, the selection of the simplest possible CFD configuration (2-D axisymmetric with swirl) leads to a good agreement with the 0-D mass flow-rate results, succeeding in an efficient hybrid computation.
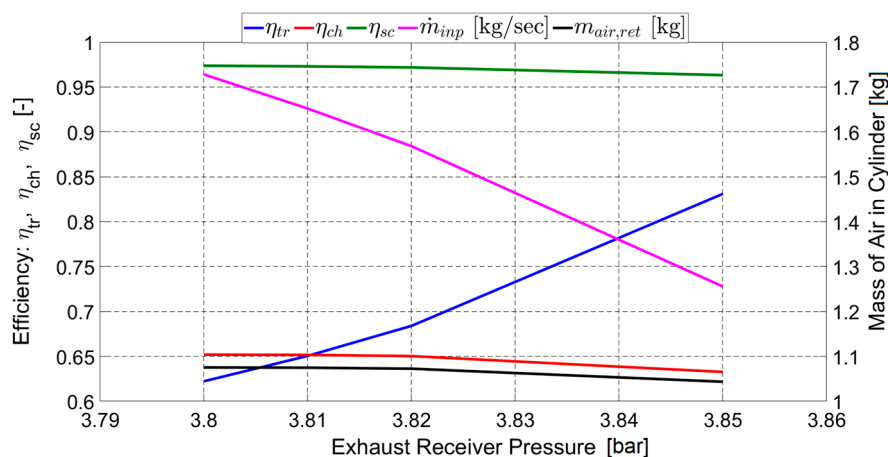

Figure 5. Effect of Δp on scavenging efficiency and mass of air entering the cylinder (100% load).

As regards validation of the flow and temperature field, the amount of validation data for a CFD model of a full size operating two-stroke marine engine is limited because of the high cost, size, and manpower required for such experiments [30]. Nevertheless, existing data from similar engines have been employed for validation, with the necessary adaptations made according to the similarity laws. As regards the validation process for the flow field, Figure 6 shows a comparison with literature data on steady state, cold flow measurements with Particle Image Velocimetry on an engine cylinder with D = 190 mm and swirl number S_m = 0.33 [31]. The measurements are presented in [31] as axial and tangential (swirl) velocity components V_z and V_θ respectively as functions of radius, normalized

with the bulk flow velocity, W_b, for various axial positions. For comparison, Figure 6 presents the CFD model predictions for the normalized V_z and V_θ components at 25% load, 195 degrees CA, at the same normalized axial positions. Only one measured axial position is inserted in the graph for comparison. The computed variation of the tangential velocity component with cylinder radius have a shape similar to a Lamb–Oseen vortex, for $z/D < 2$ ($z = 0$ corresponds to the upper end level of intake ports). The vortex core is seen as a sharp linear increase from $r = 0$. The vortex then has a smooth transition to a curve proportional to $1/r$ for larger values of r [32]. Overall, the CFD computations agree with the published experimental results on similar engines [31,33].
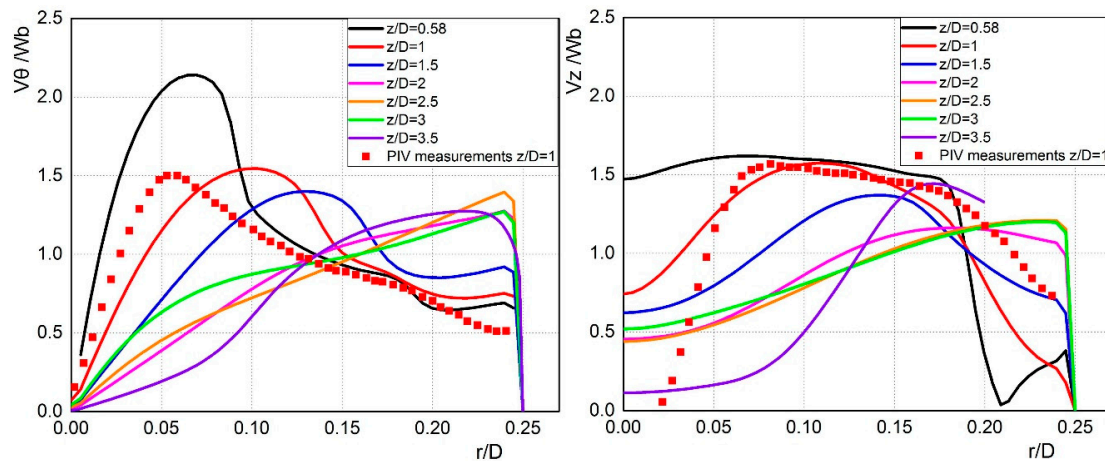
Figure 6. The mean tangential velocity component V_θ and the mean axial velocity component V_z at various axial distances from the outlet compared with PIV measurement [31].

5.3. Calculation of Zone Masses Based on CFD Results

The CFD model employed a species transport equation, which calculated a passive scalar, directly correlated to the CO_2 mass concentration in the cylinder charge. Computational cells with the highest CO_2 mass concentration are allocated to zone III and the respective cells with zero CO_2 mass concentration are allocated to zone I. The remaining volume in the cylinder corresponds to zone II. Volumes were subsequently converted to masses by employing the respective densities for air and exhaust gas. This procedure was performed at a 5 crank angle degree interval starting from 135 CA degrees (beginning of scavenging) until 225 CA degrees (end of scavenging). The mixing coefficients of the three-zone model were then revised so that results of the 0-D model would be close to results from CFD simulations.

An example of the CO_2 mass fraction evolution during scavenging is shown in Figure 7. The resulting evolution of masses for this case is shown in Figure 8. Initially, the cylinder is filled with exhaust gas. As scavenging commences, zone III continuously decreases in size, since a part of the exhaust gas leaves the cylinder through the exhaust valve and another part is transferred to the mixing zone. The mixing zone increases rapidly in the beginning of scavenging, since it receives fresh air from the air zone and exhaust gas from the exhaust gas zone. However, when the exhaust gas zone disappears, the mixing zone starts to decrease since now a part of it is escaping the cylinder through the exhaust valve. The air zone increases slowly at first, since most of the incoming air is mixed with exhaust gases, but increases faster after 180 CAD and eventually becomes larger than the mixing zone.
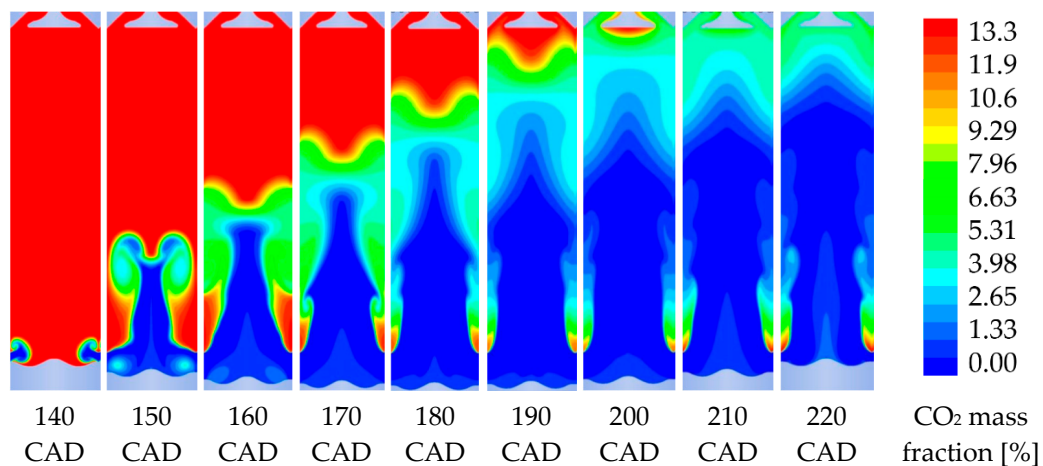
Figure 7. CO_2 mass fraction field at 10° intervals between 140–220 CAD (100% load, 10° port angle).
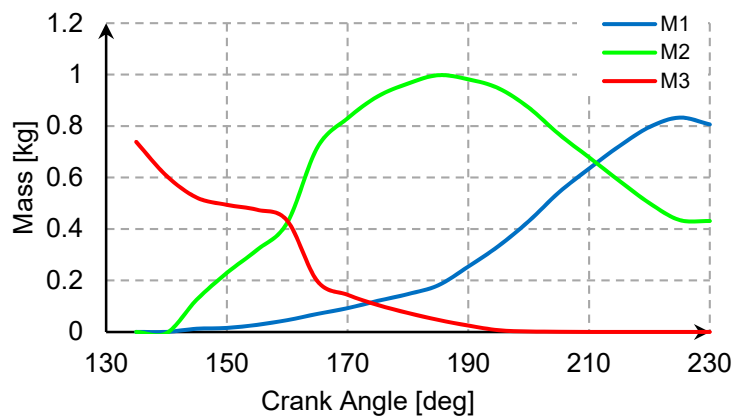

Figure 8. Evolution of the mass of each zone as predicted by the CFD model.

6. CFD Results

Results from the 2D CFD model were employed to enhance understanding of the scavenging process and update the three-zone model. The scavenging process during the time the inlet ports remain open, can be described by two processes: mixing of incoming air with exhaust gas and displacement of exhaust gas by the incoming air. The sources of mixing are:

- The jet impingement of air into the cylinder through the inlet ports
- Diffusion between exhaust gas and air at the interface between the two zones
- Flow separation at the inlet port's edges and formation of recirculation zones.

In this section, the effect of engine load, inlet port angle, and inlet port covering on scavenging will be presented.

6.1. Effect of Engine Load

Four load points that lie on a typical propeller curve passing from the MCR (maximum continuous rating) point were investigated. The propeller demand law obeys the following relation between engine speed and produced power:

$$P = c \cdot N^{\beta} \tag{13}$$

where P is engine power, N is engine speed, c is the propeller law coefficient and β usually lies between 3 and 4. Engine load influences the scavenging process in two ways. At increased load, the engine speed increases which leads to a reduced time that the inlet ports remain open. This is shown in Table 3, where scavenging time is normalized with reference to the scavenging time at 25% load.

It is observed that at 50% load scavenging time is reduced by 20%, at 75% it decreases at 70% and will further decrease at 63% when reaching 100% load. The second load dependent factor affecting scavenging is boost pressure which increases with increased engine load.

Table 3. Engine operating conditions at different load points.

Engine Load	100%	75%	50%	25%
N [RPM]	115.3	105	91.5	73
P [kW]	7620	5710	3800	1900
p_{scav} [bar]	3.90	3.15	2.20	1.48
p_{exh} [bar]	3.80	3.08	2.15	1.45
Δp [bar]	0.1	0.07	0.05	0.03
ρ_{scav} [kg/m^3]	4.34	3.54	2.47	1.66
Scavenging time with reference to 25% load	0.63	0.7	0.8	1

Since, scavenge temperature remains relatively invariable, due to the presence of the scavenge air cooler, increased scavenge pressure leads to increased air density. According to [11] mixing of air with exhaust gas increases with increased engine load due to the increased difference in density between the two gases. This is also confirmed in Figure 9 for two CA instances, 175 and 210 CAD.

In both cases mixing between air and exhaust gas is more intense for higher engine load (larger green area in Figure 9) and air manages to displace a smaller amount of exhaust gas (blue area ends at a lower axial position). A recirculation zone is formed at the cylinder wall above the scavenge ports, where pockets of exhaust gas are trapped between zones of fresh air. These pockets increase in size with increasing engine load, thus more exhaust gas is mixed with the incoming fresh air with increasing engine load in this configuration.
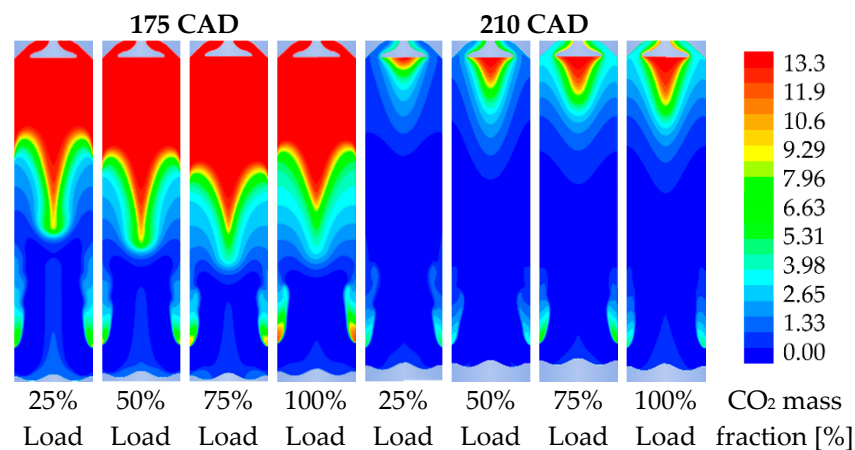
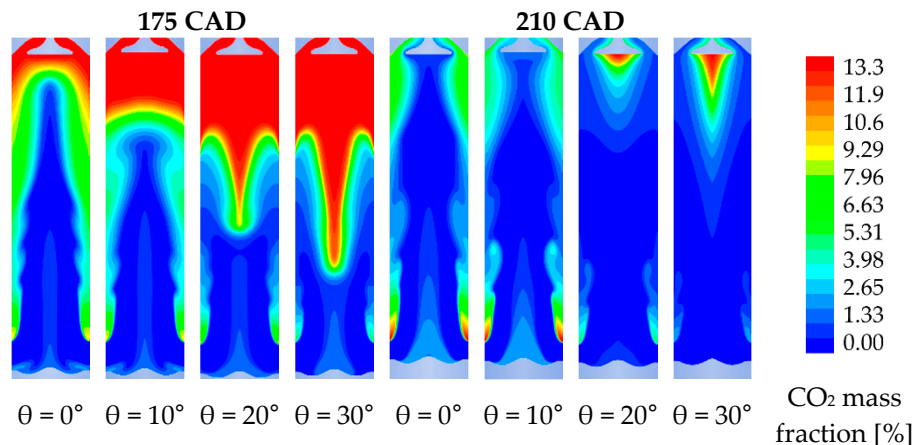**Figure 9.** CO_2 mass fraction field at 175 and 210 CAD for the four available engine loads ($\theta = 20°$).

6.2. Effect of Inlet Port Angle

Inlet ports are inclined with respect to the local radius, in order to induce a tangential component to the flow entering the engine cylinders. This creates turbulence which is beneficial for the mixing of fuel with scavenge air. The swirl could also reduce the recirculation zones that are formed near the inlet ports due to flow separation. Moreover, the cold scavenge air cools the cylinder liner and the exhaust valve. Increased in-cylinder swirl increases the tangential velocity at the cylinder liner and as a result increases the convective heat transfer coefficient.

Four port inclination angles were investigated: $\theta = 0°$, $10°$, $30°$, and $20°$ which is the industry standard. The geometric swirl number Ω was used to quantify the port induced swirl [12].

$$\Omega = \frac{A_{cyl}}{n_{inp}A_{inp}}\tan(\theta) \tag{14}$$

where A_{cyl} is the cross-sectional area of the cylinder, A_{inp} is the area of one scavenge port and n_{inp} is the number of scavenge ports. Visualization for 25% engine load and various port angles is shown in Figure 10. As expected, for $\theta = 0°$, a jet-like flow develops, which at 175 CAD (40 CAD after the beginning of scavenging) has reached the top of the cylinder. The jet is surrounded by a mixing zone located near the cylinder liner wall. As the port angle and induced swirl increases, the fresh air front moves from the cylinder axis towards the liner walls forming a V-shaped air front.

Figure 10. CO_2 mass fraction field at 175 and 210 CAD for the four investigated port angles (25% load).

As far as mixing is concerned, it is observed that larger values of port angle favour the mixing of air with exhaust gas (air penetration to the mixing zone) but hinder the penetration of exhaust gas to the mixing zone. This is in accordance with the findings of [12]. This is also verified by the masses calculated by the CFD model. As the port angle increases the mass in zone I increases slower (see Figure 11), since it loses more air to the mixing zone, while the zone III mass decreases slower, since less exhaust gas is transferred to the mixing zone.
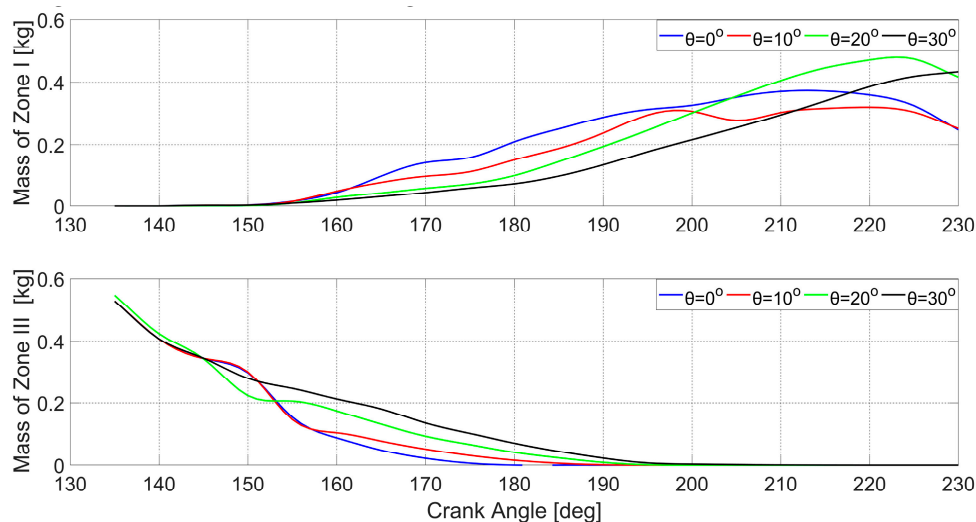
Figure 11. Evolution of mass of air zone and exhaust gas zone for various port angles at 50% load.

6.3. Effect of Inlet Port Covering in Part by the Piston Crown

The covering of the inlet ports by the piston results in an increase of the velocity of the air entering the cylinder. As a result, the jet-like nature of incoming flow is enhanced. This results in the formation

of exhaust gas recirculation zones at the sharp edges of the inlet ports, where pockets of exhaust gas are trapped within fresh air. Hence, mixing of air with exhaust gas is increased due to port covering.

On the contrary, increased port covering does not favour the entrainment of exhaust gas to the mixing zone. In Figure 12, at 210 CAD the exhaust gas zone (red zone) is slightly larger for increased inlet port covering. This is seen also in Figure 13 where the evolution of zones I and III masses is presented for the 25% load case and variable inlet port covering. Zone I increases more slowly when inlet ports are partly covered by the piston due to increased entrainment of air to the mixing zone. On the other hand, the mass of zone III decreases at a slower rate when inlet ports are partly covered since in this case mixing is retarded.
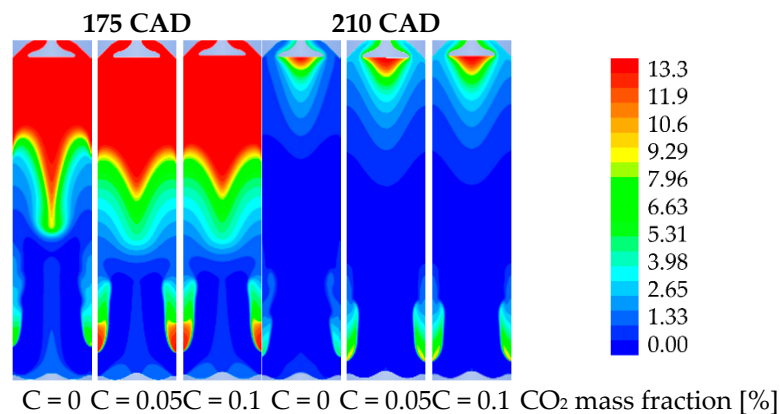
Figure 12. CO_2 mass fraction field at 175 and 210 CAD for the three investigated inlet port coverings (25% engine load and 20° port angle).
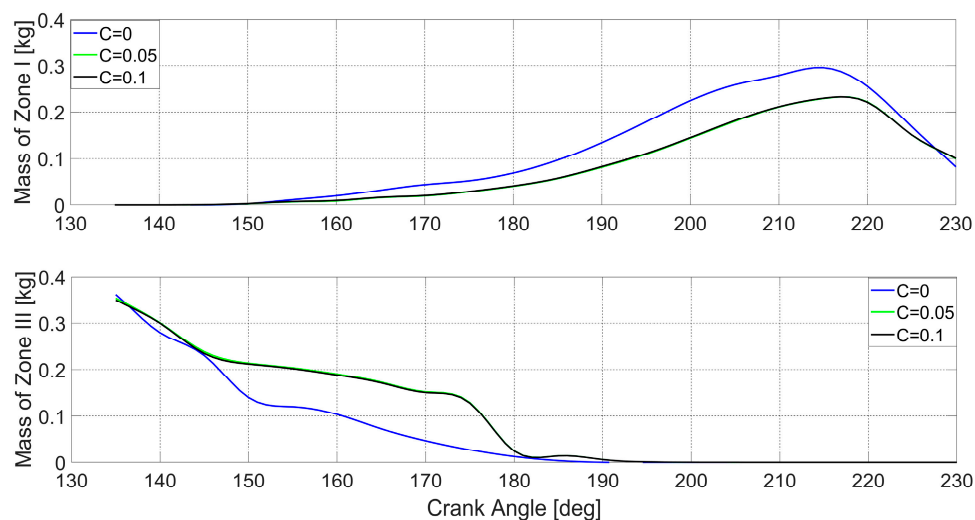
Figure 13. Evolution of mass of air zone and exhaust gas zone for various port coverings at 25% load.

As Figures 12 and 13 show, no notable differences between the 5% and 10% covering can be identified for the 25% load case.

7. The Updated Three-Zone Scavenging Model

In this section, the expressions for the evolution of the air and gas penetration coefficient for the two investigated cases will be presented. The case of varying port angle will be designated as Case I. The case of varying inlet port covering by the piston will be designated as Case II.
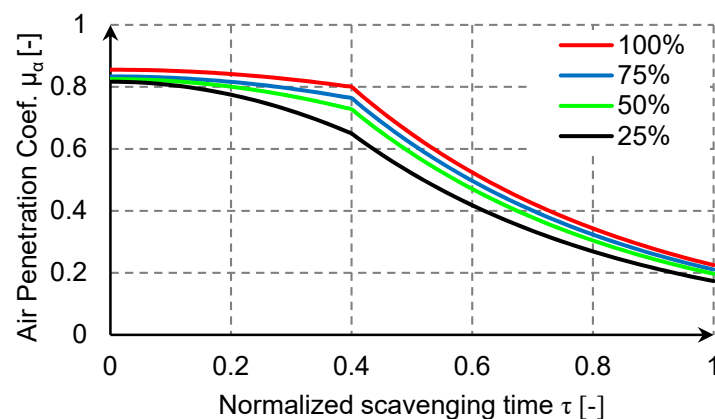
7.1. Air Penetration Coefficient

In the three-zone model, it is assumed that scavenging happens in two phases. In the first phase, when scavenge air rushes in engine cylinders, air is rapidly mixed with exhaust gases and the mixing mechanism is dominant. Hence, during the first phase the air penetration coefficient, μ_α has a large value which decreases slowly. During the second phase, displacement becomes the dominant mechanism of scavenging and μ_α decreases exponentially. The mathematical expression of the air penetration coefficient is shown below:

$$\mu_\alpha = \begin{cases} a\tau^2 + b, & 0 < \tau < \tau_a^* \\ \mu_\alpha(\tau_a^*) \exp\left(-\ln\left(\frac{\mu_\alpha(\tau_a^*)}{d}\right)(\tau_1)\right), & 0 < \tau_1 < 1 \end{cases} \tag{15}$$

where τ_1 is normalized scavenging time for the second phase of mixing of air, defined as:

$$\tau_1 = \frac{\varphi - \varphi_{\text{EFP}}}{\varphi_{\text{IPC}} - \varphi_{\text{EFP}}} \tag{16}$$

Also, a, b, and d are model parameters and τ_a^* is the time where second mixing phase begins. The evolution of the air penetration coefficient as a function of normalized scavenging time τ for different engine load points is shown in Figure 14.

Figure 14. Air penetration coefficient evolution for different engine load points ($\theta = 20°$ and C = 0).

The mathematical expression of each model parameter is given below. The expressions were produced using non-linear regression fitting. The coefficients of each equation were produced using iterative least square estimations.

7.1.1. Parameter a

This parameter, expresses the rate of decrease of mixing coefficient during the first phase of scavenging. It increases with increased engine load and port covering and decreases with increased port angle. This means that during the first phase of scavenging, mixing decreases more rapidly with increased port angle and slower for increased engine load and port covering.

$$\text{(I) } a = \begin{cases} 0.03 - 0.37\left(\frac{N}{N_{\text{mcr}}}\right)^{-2.2}, & \theta \in [10, 30] \\ 0, & \theta \in [0, 10] \end{cases} \tag{17}$$

$$\text{(II) } a = 1.1 - 1.42\left(\frac{N}{N_{\text{mcr}}}\right)^{-0.8} + 0.5 \cdot C^{0.2} \tag{18}$$

7.1.2. Parameter b

Model parameter b, expresses the initial value of the mixing coefficient during IPO. This parameter was found to be increasing with increasing with engine load, port angle and port covering.

$$\text{(I) b} = 0.8 - 0.05\left(\frac{N}{N_{mcr}}\right)^{-1.5} + 0.2\cdot\Omega^{0.8} \tag{19}$$

$$\text{(II) b} = 2.8 - 1.9\left(\frac{N}{N_{mcr}}\right)^{-0.1} + 0.5\cdot C \tag{20}$$

7.1.3. Parameter d

This parameter, expresses how steep the exponential decline of the air penetration coefficient is. It was observed to increase with engine load and port covering and decrease with increased inlet port angle. This means that with increased engine load and port covering, μ_α decreases slower, while as inlet port angle increases μ_α decreases more rapidly.

$$\text{(I) d} = 0.28 + 0.035\left(\frac{N}{N_{mcr}}\right)^{2.5} - 0.29\cdot\Omega^{0.35} \tag{21}$$

$$\text{(II) d} = 0.1\left(\frac{N}{N_{mcr}}\right)^{2.2} + 0.16\cdot C^{0.1} \tag{22}$$

7.1.4. Parameter τ_a^*

Parameter τ_a^* expresses the time instant when the second mixing phase commences. This parameter was found to increase with port angle, and be independent of engine load or inlet port covering.

$$\text{(I) } \tau_a^* = 0.27 + 0.3\cdot\Omega^{0.7} \tag{23}$$

$$\text{(II) } \tau_a^* = 0.42, \ \forall\, C \tag{24}$$

7.2. Gas Penetration Coefficient

The model assumes that the entrainment of exhaust gases to the mixing zone is divided in two phases. In the first phase, the evolution of mixing resembles the one of entrainment of ambient fluid into jets and increases parabolically. The initial phase of increasing mixing will be terminated due to jet interaction and confinement as well as due to the displacement of the exhaust gas. In the second phase, mixing of exhaust gas decreases and μ_g drops exponentially. The mathematical expression of μ_g is shown in Equation (25), where σ and k_g are model parameters and τ_2. is normalized scavenging time of the second mixing phase.

$$\mu_g = \begin{cases} \sigma\sqrt{\dfrac{\tau}{\tau_g^*}}, & 0 < \tau < \tau_g^* \\ e^{-k_g(\tau_2)}\mu_g\left(\tau_g^*\right)(1 + \tau_2), & 0 < \tau_2 < 1 \end{cases} \tag{25}$$

The duration of the first mixing phase τ_g^*. was estimated at 15–20% of total scavenging time hence, $\tau_g^* = 0.17$. . The evolution of the gas penetration coefficient as a function of normalized scavenging time τ for different engine load points is shown in Figure 15.
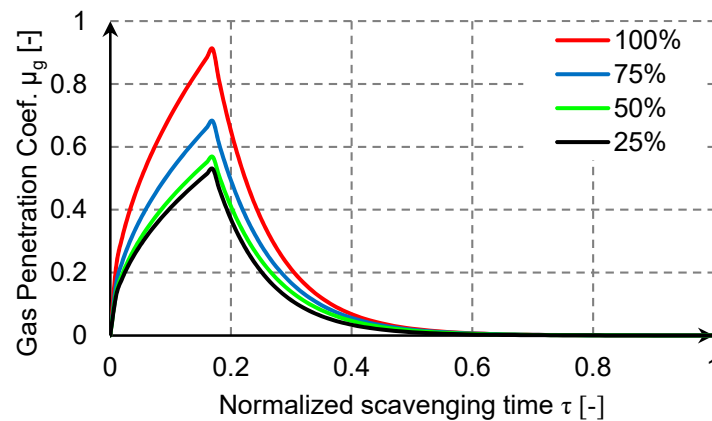
Figure 15. Gas penetration coefficient evolution for different engine load points ($\theta = 20°$ and $C = 0$).

In reality, the transition from one mixing phase to the next, that takes place in τ_g^* would be quite smoother. However, the presented expression was preferred since it provided a better prediction of the evolution of each mass.

7.2.1. Parameter σ

This parameter expresses the peak value of the gas penetration coefficient during the first phase of mixing. Increased values of σ indicate increased mixing of exhaust gas. Since mixing increases with load, σ also increases with load. On the other hand, for increased inlet port angle, the recirculation zones that are formed act as a barrier towards the entrainment of exhaust gas to the mixing zone [9]. As a result, σ decreases with increased port angle. As far as port covering by the piston is concerned, σ decreases with port covering, since port covering was found to hinder the entrainment of exhaust gas to the mixing zone.

$$(I) \ \sigma = 0.75 + 0.4\left(\frac{N}{N_{mcr}}\right)^5 - 0.7{\cdot}\Omega \tag{26}$$

$$(II) \ \sigma = 0.45 + 0.4\left(\frac{N}{N_{mcr}}\right)^5 - 0.6{\cdot}C^{0.4} \tag{27}$$

7.2.2. Parameter k_g

Model parameter k_g expresses how rapidly the entrainment of exhaust gas to the mixing zone declines. Increased values of k_g indicate decreased mixing. This parameter increased with engine load and port angle and decreased with inlet port covering.

$$(I) \ k_g = 6.5 + 0.5\left(\frac{N}{N_{mcr}}\right)^3 + 5{\cdot}\Omega^{0.5} \tag{28}$$

$$(II) \ k_g = 10.5 + \left(\frac{N}{N_{mcr}}\right)^4 + 2{\cdot}C^{0.6} \tag{29}$$

8. Validation of the Updated Three-Zone Model Against CFD Results

The revised zero-dimensional three-zone model was validated against results from CFD simulations. The predicted masses at each zone using the updated 0-D model were compared to the masses predicted by the 2-D CFD model. Validation results are presented in Figures 16 and 17 where CFD results are presented with solid line and results of the updated 0-D model are presented with dashed line. In both cases, the updated model manages to accurately predict the qualitative evolution of scavenging, as predicted by the CFD model. In both presented cases the updated 0-D

model slightly overestimates the mass of the air zone and predicts the dissipation of the exhaust gas zone slightly faster than the CFD model.
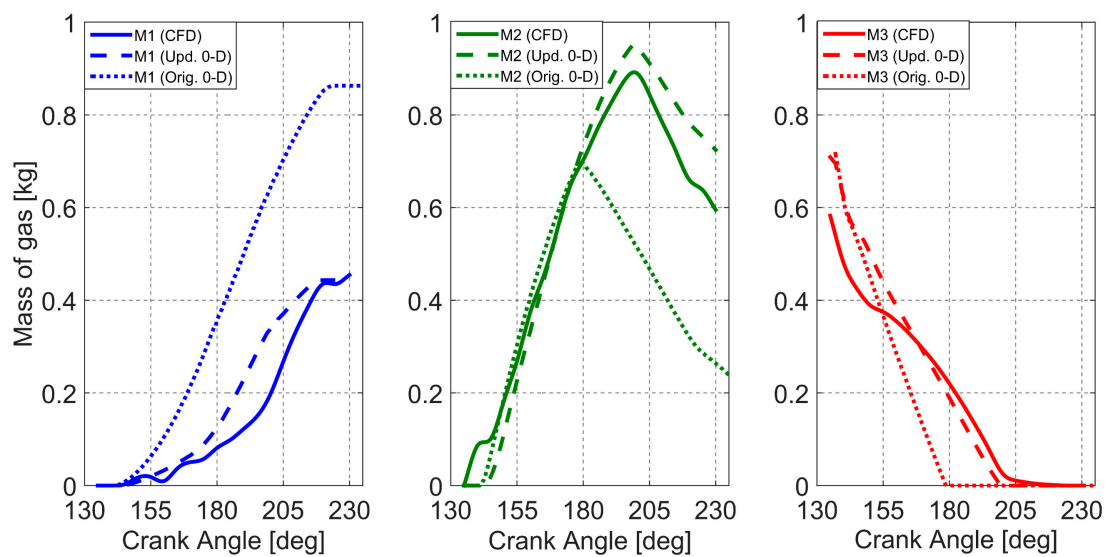
Figure 16. Evolution of mass of each zone as predicted by the original 0-D model, the updated 0-D model and the CFD model for the 75% load, θ = 20°, C = 0.1 case.
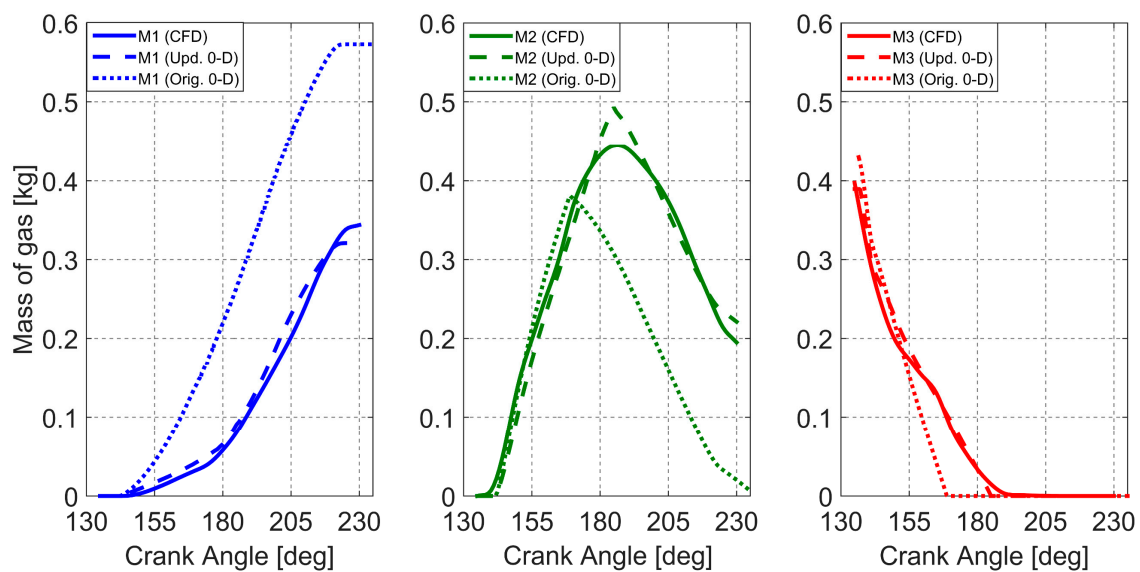
Figure 17. Evolution of mass of each zone as predicted by the original 0-D model, the updated 0-D model and the CFD model for the 25% load, θ = 30°, C = 0 case.

Results of the original 0-D model are also included in the graphs (dotted line) for comparison. In both cases, the original model significantly overestimates the evolution of zone I. This means that the original model predicts that less amount of air is mixed with exhaust gases, than the one predicted by the CFD model. Moreover, the original model predicts that the dissipation of zone III takes place about 20 CAD earlier than the CFD. As far as the mixing zone is concerned, results from the original model are close to the ones from CFD simulations until the dissipation of zone III takes place. Once this happens, the mixing zone begins to reduce rapidly and the original 0-D model results deviate significantly from CFD simulation results. The amount of gas that remains in the engine cylinder at the end of scavenging (235 CAD) is very close in both cases.

9. Conclusions

An updated zero-dimensional three-zone model for the simulation of the scavenging process of uniflow scavenged two-stroke diesel engines was presented. In order to gain insight on the scavenging process of the engine and update the model, a CFD model of a large two-stroke marine diesel engine was used. The updated model, takes into account the effect of engine load, port angle, and inlet port covering on the scavenging process. Each of the three zones of the model (air zone, mixing zone and exhaust gas zone), is considered as a control volume. The entrainment of air and exhaust gas in the mixing zone is specified through time varying mixing coefficients. The influence of the different scavenging mechanisms was implicitly taken into account by considering the scavenging process to constitute two different phases. CFD simulations showed that mixing of air with exhaust gas increased with increased engine load. Moreover, increasing inlet port-induced swirl and inlet port covering were found to increase the entrainment of air to the mixing zone but decrease the entrainment of exhaust gases to the mixing zone. These results were compatible with the findings of previous works such as [9,11,12]. The updated three-zone model can be used in conjunction with an engine performance prediction code to simulate the performance and especially the transient exhaust gas temperature of a modern uniflow scavenged two stroke large marine diesel engine. The described updating procedure enabled a higher accuracy of the 0-D model, without increasing the computational time and the complexity, by taking into account the gas flow in the cylinder through detailed CFD simulations. The future objective of this work is to be able to investigate with better accuracy the transient response of such a marine engine with a coupled SCR aftertreatment system when driving a propeller of a ship in heavy weather.

Nomenclature

A	Area, m^2
a	Air penetration coefficientarameter
BDC	Bottom de center
b	Air penetration coefficientarameter
C	Percentage of the inlet port area covered by the piston own
CAD	Crank ang degrees
c	Propeller law coefficient
d	Air penetration coefficientarameter
EGR	Exhaust gas recirculation
h	Specific enthalpy, J/kg
IPO	Inlet port oning
k_g	Gas penetration coefficient parameter
$\dot{m}$	Mass flow rate, kg/sec
MCR	Maximum continuous rating, kW
N	Engine rotational speed, RPM
n_{inp}	Number of inlet ports
p	Pressure, r

P	Power, kW
Q	Heat flow, J
S_m	Swirl number
SCR	Selective catalytic reduction
T	Temperature, K
TDC	Top dead center
u	Specific energy, J/kg
V	Volume, m^3
V_θ	Tangential velocity component, m/s
V_z	Axial velocity component, m/s
W_b	Mean velocity at the axial position, m/s

Greek Characters

β	Propeller law exponent
η_{ch}	Charging efficiency
η_{sc}	Scavenging efficiency
η_{tr}	Trapping efficiency
θ	Inlet port angle, °
κ	Constant of the original three-zone model
λ	Constant of the original three-zone model
μ	Mixing coefficient
ξ	Constant of the original three-zone model
ρ	Density, kg/m^3
σ	Gas penetration coefficient parameter
τ	Dimensionless scavenging time
τ_1	Normalized scavenging time for second phase of mixing of air
τ_2	Normalized scavenging time for second phase of mixing of burnt gas
τ_a^*	End of first mixing phase for the air
τ_g^*	End of first mixing phase for the exhaust gas
φ	Crank angle, °
Ω	Geometric swirl numr

Subscripts

a	Air
air, ret	Airetained
air, del	Air delivered
tr	Trapped cylinder charge
cyl	Cylinder
EBF	End of backflow
EFP	End of first mixing phase
exh	Exhst receiver
exv	Exhaust valve
g	Exhaust Gas
IPC	Inlet port closing
j	Different entries to the control volume
MCR	Maximum continuous rating, kW
scav	Scavenge receiver
sf	Surfaces with different rates of heat traner
inp	Inleports

References

1.　MAN Diesel & Turbo. *MAN B&W S50MC-C8.2 Tier II Project Guide*; MAN Diesel & Turbo: Copenhagen, Denmark, 2014.
2.　Ferro, A. Investigation by means of models into the scavenging of the two-stroke internal combustion engines. *Eng. Dig.* **1958**, *19*, 512–522.

3. Percival, W.H. Method of Scavenging Analysis for 2-Stroke-Cycle Diesel Cylinders. *SAE Trans.* **1995**, *63*, 737–751. [CrossRef]

4. Sher, E.; Hossain, I.; Zhang, Q.; Winterbone, D. Calculations and measurements in the cylinder of a two-stroke uniflow-scavenged engine under steady flow conditions. *Exp. Therm. Fluid Sci.* **1991**, *4*, 418–431. [CrossRef]

5. Litke, B. The influence of inlet angles in inlet ports on the scavenging process in two-stroke uniflow-scavenged engine. *Trans. Built Environ.* **1999**, *45*, 247–252.

6. Wang, X.; Ma, J.; Zhao, H. Analysis of scavenge port designs and exhaust valve profiles on the in-cylinder flow and scavenging performance in a two-stroke boosted uniflow scavenged direct injection gasoline engine. *Int. J. Engine Res.* **2017**, *19*, 509–527. [CrossRef]

7. Sher, E. Scavenging the two-stroke engine. *Prog. Energy Combust. Sci.* **1990**, *16*, 95–124. [CrossRef]

8. Heywood, J.B.; Sher, E. *Two-Stroke Cycle Engine: It's Development, Operation and Design*; Taylor & Francis Group: New York, NY, USA, 1999.

9. Sigurdsson, E.; Ingvorsen, K.; Jensen, M.; Mayer, S.; Matlok, S.; Walther, J. Numerical analysis of the scavenge flow and convective heat transfer in large two-stroke marine diesel engines. *Appl. Energy* **2014**, *123*, 37–46. [CrossRef]

10. Lamas, M.; Vidal, C.G.R. Computational Fluid Dynamics Analysis of the Scavenging Process in the MAN B&W 7S50MC Two-Stroke Marine Diesel Engine. *J. Ship Res.* **2012**, *56*, 154–161.

11. Andersen, F.H.; Mayer, S. Parametric Study of the Scavenging Process in Marine Two-Stroke Diesel Engines. In Proceedings of the ASME Internal Combustion Engine Division Fall Technical Conference, Houston, TX, USA, 8–11 November 2015.

12. Andersen, F.H.; Hult, J.; Nogenmyr, K.-J.; Mayer, S. CFD Analysis of the Scavenging Process in Marine Two-Stroke Diesel Engines. In Proceedings of the ASME Internal Combustion Engine Division Fall Technical Conference, Columbus, IN, USA, 19–22 October 2014.

13. Sigurdsson, E. Scavenging Flow in a Two-Stroke Diesel Engine. Master's Thesis, Technical University of Denmark, Copenhagen, Denmark, 2011.

14. Obeidat, A.; Schnipper, T.; Ingvorsen, K.M.; Haider, S.; Meyer, K.E.; Mayer, S.; Walther, J.H. Large eddy simulations of the influence of piston position on the swirling flow in a model two-stroke diesel engine. *Int. J. Numer. Methods Heat Fluid Flow* **2014**, *24*, 325–341. [CrossRef]

15. Kyrtatos, N.P.; Koumbarelis, I. A three-Zone scavenging model for two-stroke uniflow engines. *J. Eng. Gas Turbines Power* **1988**, *110*, 531–537. [CrossRef]

16. Foteinos, M.; Konstantinidis, S.; Kyrtatos, N.; Busk, K.V. Simulation of the transient thermal response of a high pressure SCR aftertreatment system for a Tier III two-stroke marine diesel engine ASME. *J. Eng. Gas Turbines Power* **2019**, *141*. [CrossRef]

17. Llamas, X.; Eriksson, L. Control-oriented modeling of two-stroke diesel engines with EGR for marine applications. *Proc. Inst. Mech. Eng. Part M J. Eng. Marit. Environ.* **2018**, 1–24. [CrossRef]

18. Chybowski, L.; Laskowski, R.; Gawdzińska, K. An overview of systems supplying water into the combustion chamber of diesel engines to decrease the amount of nitrogen oxides in exhaust gas. *J. Mar. Sci. Technol.* **2015**, *20*, 393–405. [CrossRef]

19. Kyrtatos, N.; Koumbarelis, I. Performance prediction of next generation slow speed diesel engines during ship manoeuvres. *Trans. Inst. Mar. Eng.* **1994**, *106*, 1–26.

20. Livanos, A.; Theotokatos, G.; Kyrtatos, N. Simulation of large marine two-stroke diesel engine operation during fire in the scavenging air receiver. *J. Mar. Eng. Technol.* **2003**, *A3*, 9–16. [CrossRef]

21. Theotokatos, G.; Kyrtatos, N.P. Diesel engine transient operation with turbocharger compressor surging. In Proceedings of the SAE 2001 World Congress, Detroit, MI, USA, 5–8 March 2001.

22. Kyrtatos, N.; Theotokatos, G.; Xiros, N.; Marec, K.; Duge, R. Transient operation of large-bore two-stroke marine diesel engine powerplants: measurements and simulations. In Proceedings of the 23rd CIMAC World Congress, Hamburg, Germany, 7–10 May 2001.

23. Anderson, J.D. *Computational Fluid Dynamics*; McGraw-Hill: New York, NY, USA, 1995.

24. Ferziger, J.H.; Peric, M. *Computarional Methods for Fluid Dynamics*; Springer: New York, NY, USA, 2002.

25. ANSYS, Inc. *ANSYS Fluent Theory Guide (Release 15.0)*; ANSYS, Inc.: Canonsburg, PA, USA, 2013.

26. ANSYS, Inc. *ANSYS ICEM CFD User's Manual (Release 17.0)*; ANSYS Inc.: Canonsburg, PA, USA, 2016.

27. Foteinos, M.I.; Tzanos, E.I.; Kyrtatos, N.P. Ship Hull Fouling Estimation Using Shipboard Measurements, Models for Resistance Components, and Shaft Torque Calculation Using Engine Model. *J. Ship Res.* **2017**, *61*, 64–74. [CrossRef]

28. Kyrtatos, N.; Tzanos, E.; Coustas, J.; Vastarouhas, D.; Rizos, E. Shipboard engine performance assessment by comparing actual measured data to nominal values produced by detailed engine simulations. In Proceedings of the CIMAC Congress, Bregen, Norway, 14–17 June 2010.

29. Kyrtatos, N.; Glaros, S.; Tzanos, E.; Hatzigrigoris, S.; Dalmyras, F. Systematic evaluation of performance of VLCC engine, comparing service monitored data and thermodynamic model predictions. In Proceedings of the 27th CIMAC World Congress on Combustion Engine Technology, Shanghai, China, 13–16 May 2013.

30. Andersen, F.H. *Integrated Analysis of the Scavenging Process in Marine Two-Stroke Diesel Engines*; DTU Mechanical Engineering: Copenhagen, Denmark, 2015.

31. Ingvorsen, K.M.; Meyer, K.E.; Schnipper, T.; Jens, H.; Mayer, S. Swirling flow in model of large two-stroke diesel engine. In Proceedings of the 16th International Symposium on Applications of Laser Techniques to Fluid Mechanics, Lisbon, Portugal, 9–12 July 2012.

32. Luca-Negro, O.; Doherty, T.O. Vortex breakdown: A review. *Prog. Energy Combust. Sci.* **2001**, *27*, 431–481. [CrossRef]

33. Haider, S.; Schnipper, T.; Obeidat, A.; Meyer, K.E.; Okulov, V.L.; Mayer, S.; Walther, J.H. PIV study of the effect of piston position on the in-cylinder swirling flow during the scavenging process in large two-stroke marine diesel engines. *J. Mar. Sci. Technol.* **2013**, *18*, 133–143. [CrossRef]